Hindawi Publishing Corporation
International Journal of Geophysics
Volume 2011, Article ID 958483, 16 pages
doi:10.1155/2011/958483

Research Article

Advantages of Shear Wave Seismic in Morrow Sandstone Detection

Paritosh Singh and Thomas Davis

Colorado School of Mines, Golden, CO 80401-1843, USA

Correspondence should be addressed to Paritosh Singh, psingh@mymail.mines.edu

Received 25 December 2010; Accepted 7 March 2011

Academic Editor: Yu Zhang

The Upper Morrow sandstones in the western Anadarko Basin have been prolific oil producers for more than five decades. Detection of Morrow sandstones is a major problem in the exploration of new fields and the characterization of existing fields because they are often very thin and laterally discontinuous. Until recently compressional wave data have been the primary resource for mapping the lateral extent of Morrow sandstones. The success with compressional wave datasets is limited because the acoustic impedance contrast between the reservoir sandstones and the encasing shales is small. Here, we have performed full waveform modeling study to understand the Morrow sandstone signatures on compressional wave (P-wave), converted-wave (PS-wave) and pure shear wave (S-wave) gathers. The contrast in rigidity between the Morrow sandstone and surrounding shale causes a strong seismic expression on the S-wave data. Morrow sandstone shows a distinct high amplitude event in pure S-wave modeled gathers as compared to the weaker P- and PS-wave events. Modeling also helps in understanding the adverse effect of interbed multiples (due to shallow high velocity anhydrite layers) and side lobe interference effects at the Morrow level. Modeling tied with the field data demonstrates that S-waves are more robust than P-waves in detecting the Morrow sandstone reservoirs.

1. Introduction

The Anadarko Basin is one of the major hydrocarbon producing provinces in the USA. According to Sorenson [1], Panhandle-Hugoton field in Western Anadarko Basin is a giant oil field (estimated ultimate recovery (EUR) 1400 million bbl of oil) and the largest conventional gas field in North America (EUR > 75 tcf). Hydrocarbon production in the Anadarko basin is mainly from three geologic zones—the Upper Mississippian and Pennsylvanian sandstones, Permian carbonates, and Mississippian carbonates [2]. Permian Council Grove and Chase Group carbonate rock gas fields are by far the largest hydrocarbon producers in the basin. The Pennsylvanian Upper Morrow sandstone reservoir in western Anadarko Basin is a major oil-producing reservoir. It consists of multiple-stacked lenticular sandstone bodies formed within valley-fill complexes. These sandstones have confounded operators and investigators alike because of their irregular distribution. Compressional wave studies have been mostly done for characterizing the Morrow sandstones [3, 4]. It is difficult to detect these thin and discontinuous reservoir sandstones using P-wave datasets because of insufficient acoustic impedance contrast between Morrow sandstone and surrounding shales. The P-wave study is further limited since the interference effects due to side lobe of Morrow shale dominate the subtle P-wave AVO (amplitude versus offset) response [5]. Thus, P-wave seismic methods have not been successful in imaging Morrow sandstone accumulations within this valley-fill system.

Shear wave data can help improve structural imaging where P-impedance contrast is low, imaging through gas clouds, lithology and fluid estimation, fracture detection, and reservoir monitoring, which reduces risk and creates new exploration opportunities [6, 7]. Engelmark [8] showed modeling results where converted-wave imaging can be valuable when the acoustic-impedance contrast between seal and reservoir is weak. Alba Field is one of the field examples where converted-wave data has been successfully used to image low P-impedance reservoirs [9]. Margrave et al. [10] reported success interpreting channel sands with 3C data

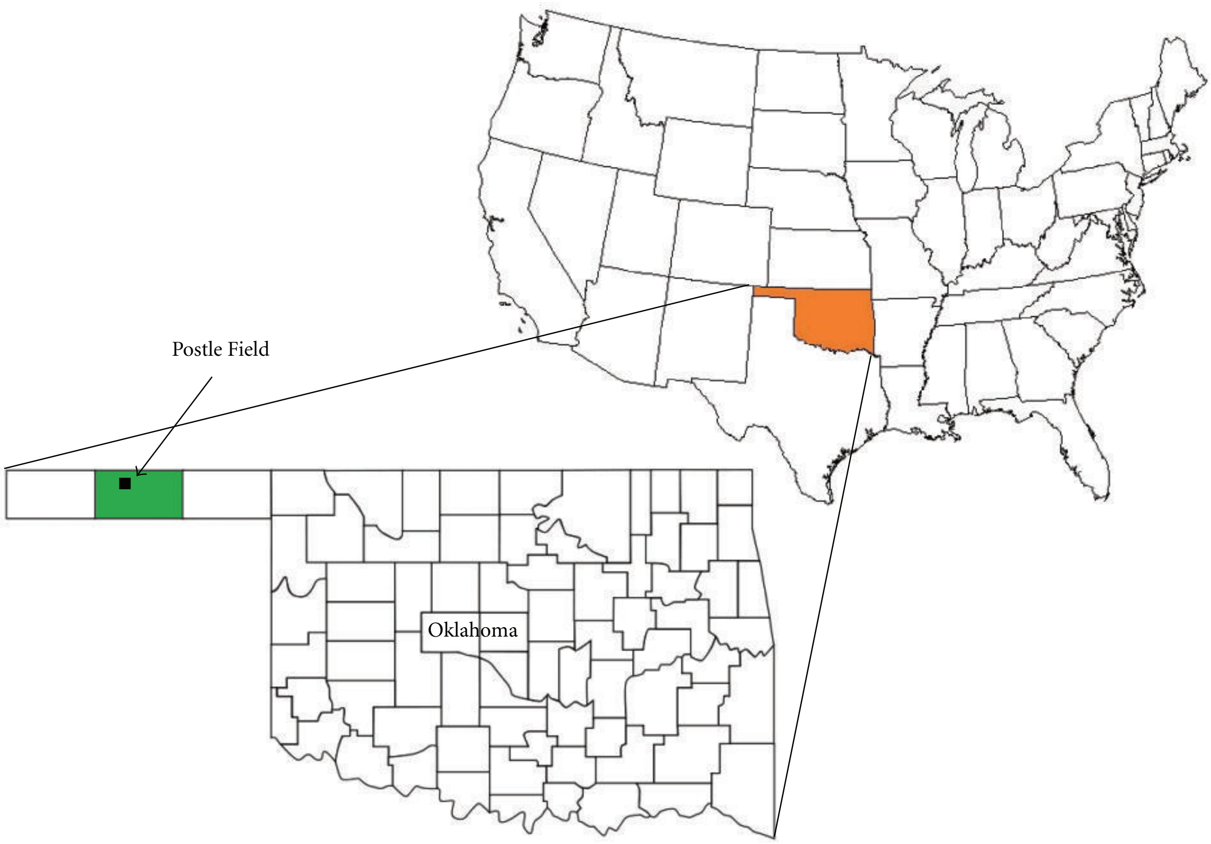

Figure 1: Location of Postle Field in Texas County, Oklahoma.

in Blackfoot Field by using V_p/V_s measurement. Knapp et al. [11] presented a case study in Gulf of Mexico to show the significance of converted-wave data in imaging through gas clouds. The importance of 4C data for lithology and fluid estimation has been showed by Engelmark [12]. Fractured reservoirs cause shear-wave birefringence as they propagate through them [13, 14]. The fast shear wave (S1) is polarized parallel to the fracture strike direction and the slow shear wave (S2) is polarized perpendicular to the dominant fracture strike direction in the symmetry axis plane. Crampin [15–18] stresses the importance of shear wave splitting phenomenon to exploration geophysics. Lynn and Thomsen [19] published one of the first field examples which demonstrate use of S-wave anisotropy in an exploration context. Mueller [20] has showed the use of S-wave splitting for Austin chalk fracture detection. Time lapse S-wave data has been used as a production-monitoring tool in unconventional reservoirs such as tight gas sandstone reservoir in Rulison Field [21] and carbonate reservoir in Weyburn Field [22].

Most of the above-mentioned studies have been done using converted-wave data. Importance of shear waves has been mostly demonstrated using PS-waves (Stewart et al. [23]) as compared to S-waves. The present study shows the value of S-wave data in imaging of Morrow sandstone reservoirs using full waveform modeling and real-data results. Study by Wilson [24] in Eva South field demonstrated that PS-waves can be successfully used for Morrow sandstone detection in an area where P-wave fails. He showed that V_p/V_s and PS1 amplitude maps improve the mapping of Morrow sandstone distribution. Blott [25] demonstrated the importance of 9C dataset in detecting the Morrow sandstones in Sorrento field by using V_p/V_s and S1 and S2 amplitude maps. Rampton [26] showed the usefulness of PS- and S-wave VSP (vertical seismic profile) data for detecting the reservoir sandstones, while verifying that compressional energy corresponds primarily to nonreservoir rock at the Morrow level. Wiley [5] indicates the presence of faults in such fields and there can be fractures associated with them in all the hydrocarbon producing geologic zones. Shear wave splitting can help in understanding these fractures and improve production.

This study is focused on Postle Field which was discovered in 1958. The production phases began with primary production, followed by water flooding in 1965 and CO_2 enhanced oil recovery from 1995. The field has produced nearly 120 million barrels or 40% of an estimated 300 million barrels of OOIP (original oil in-place) [27]. Thus, understanding the dynamics of the reservoir is very important in the design and success of the flood management in such mature fields. Multicomponent data can help in detecting the sandstone distribution and movement of CO_2 injection, since shear waves are sensitive to pressure changes and do not depend significantly on saturating fluids [28, 29].

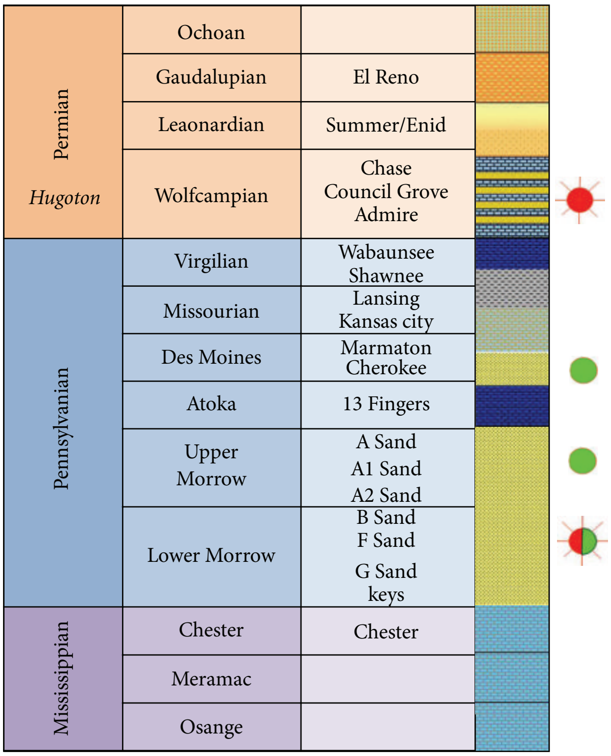

FIGURE 2: Stratigraphic column of Postle Field (courtesy Whiting Petroleum).

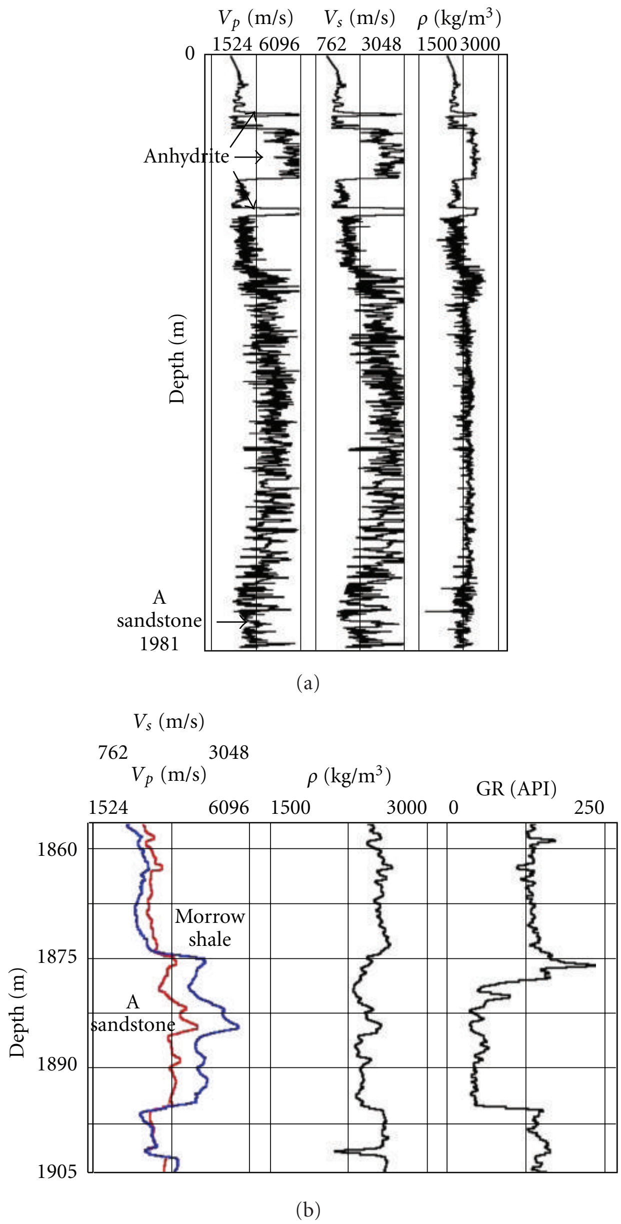

FIGURE 3: Well logs used for modeling show Morrow A sandstone at 1875 m and shallow anhydrite layers. Close-up of the Morrow interval (b) shows the strong S-wave velocity (blue curve) contrast as compared to P-wave velocity (red curve) contrast between Morrow shale and A sandstone.

The main producing reservoir in the study area is the Morrow A sandstone. It is observed that the acoustic impedance percentage difference between Morrow shales and sandstones is ~10%, whereas the shear impedance percentage difference is ~40%. We perform full waveform modeling to understand the Morrow A sandstone AVO signatures on P-wave, PS-wave and S-wave [30]. Modeling demonstrates that Morrow sandstones can be better mapped using S-wave data, whereas P-wave and PS-wave data are insufficient in imaging these sandstones. Due to low acoustic impedance contrast and interference effects, P-wave AVO has not been used until now to characterize the Morrow sandstones. But elastic modeling suggests that S-wave AVO can be of great help in characterizing these sandstones. The modeling results in combination with the field data results show that pure S-wave data can help in finding new prospects and guide in future drilling locations. This is the first study to do full waveform modeling for understanding the Morrow A sandstone response on P-, PS- and S-waves and help in multicomponent data processing and interpretation. Modeling also helps in understanding the effect of shallow anhydrite layers on data quality and this study has never been done before for Morrow sandstone reservoirs. The importance of this study is the accumulation of strong evidence demonstrating the direct detection of reservoir sandstone using S-waves. This study encourages having more S-wave seismic studies in characterizing the Morrow sandstones in such mature fields.

2. Geologic Background

The study area is located in Postle Field, Anadarko Basin, Oklahoma (Figure 1). The area is flanked in the west by the Keys dome, in the south by the Amarillo uplift and in the north by the Hugoton embayment [31]. Figure 2 provides the generalized stratigraphic column of the Postle Field and the stratigraphy of this basin has been discussed in detail by Bowen and Weimer [32] and Henry and Hester [33]. Mississippian and older rocks are mainly carbonates, whereas Pennsylvanian and younger rocks are mainly shales with

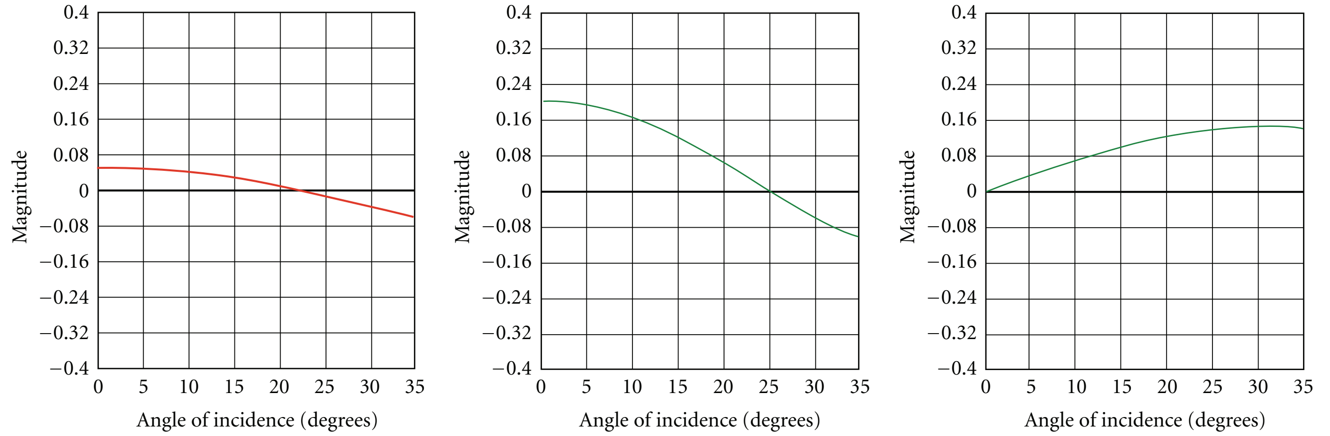

(a) P-wave AVA (b) S-wave AVA (c) PS-wave AVA

Figure 4: Amplitude versus angle (AVA) response for P-wave, S-wave, and PS-wave for the velocity contrast between Morrow shale and A sandstone shown in Figure 3.

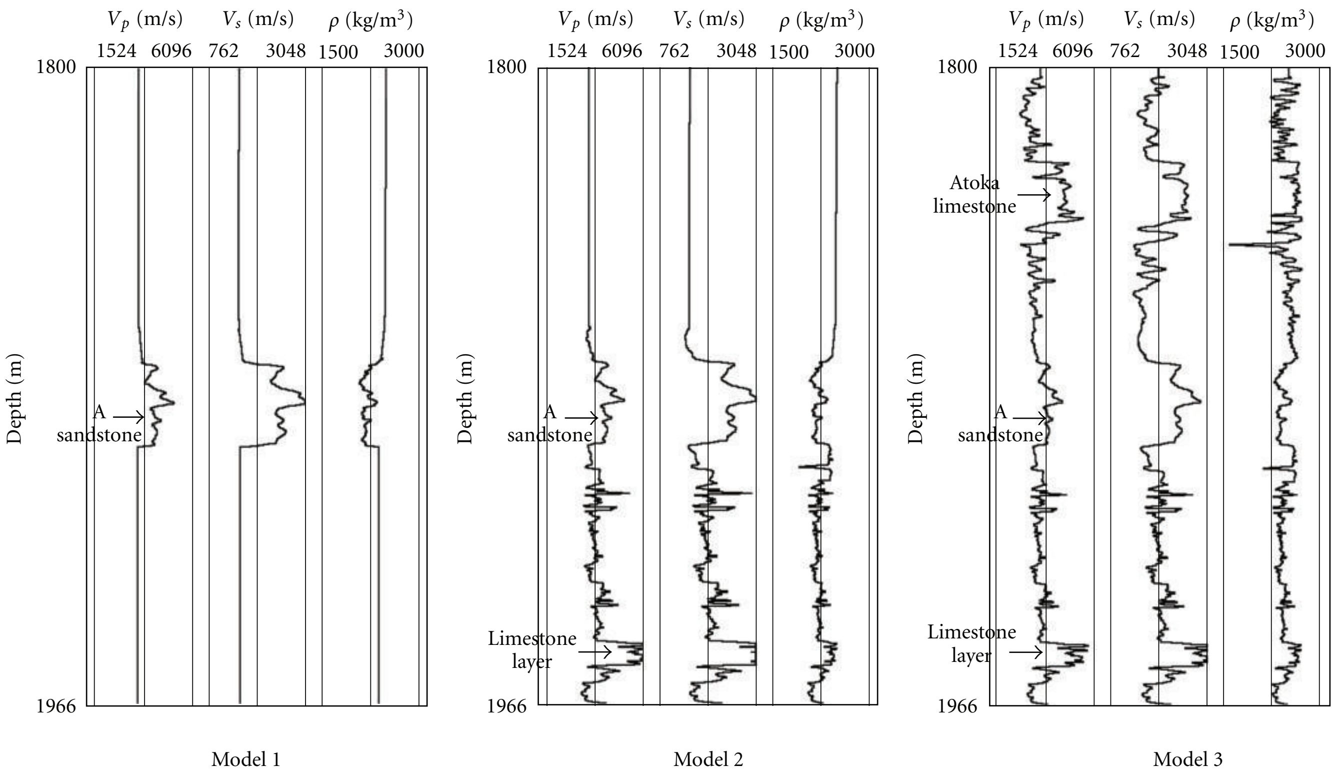

(a) (b) (c)

Figure 5: The three different 1D models used to understand the Morrow A sandstone response on synthetic gathers. Model 1—only Morrow A sandstone interval, Model 2—Morrow A sandstone with one limestone layer below, and Model 3—Morrow A sandstone with Atoka limestone above and one limestone layer below.

some sandstones. The Morrow formation lies uncoformably on top of Mississipian strata and conformably below the Thirteen Fingers limestone [34]. The Upper Morrow consists of multiple stacked lenticular sandstone bodies formed within valley fill complexes. The Morrow sandstones are major hydrocarbon producers in this basin along with the shallow Permian Council Grove and Chase Group carbonate rock gas reservoirs. The main reservoir in our study area is the Morrow A sandstone which are at a depth of around 1875 m and have an average thickness of 10 m (0–30 m).

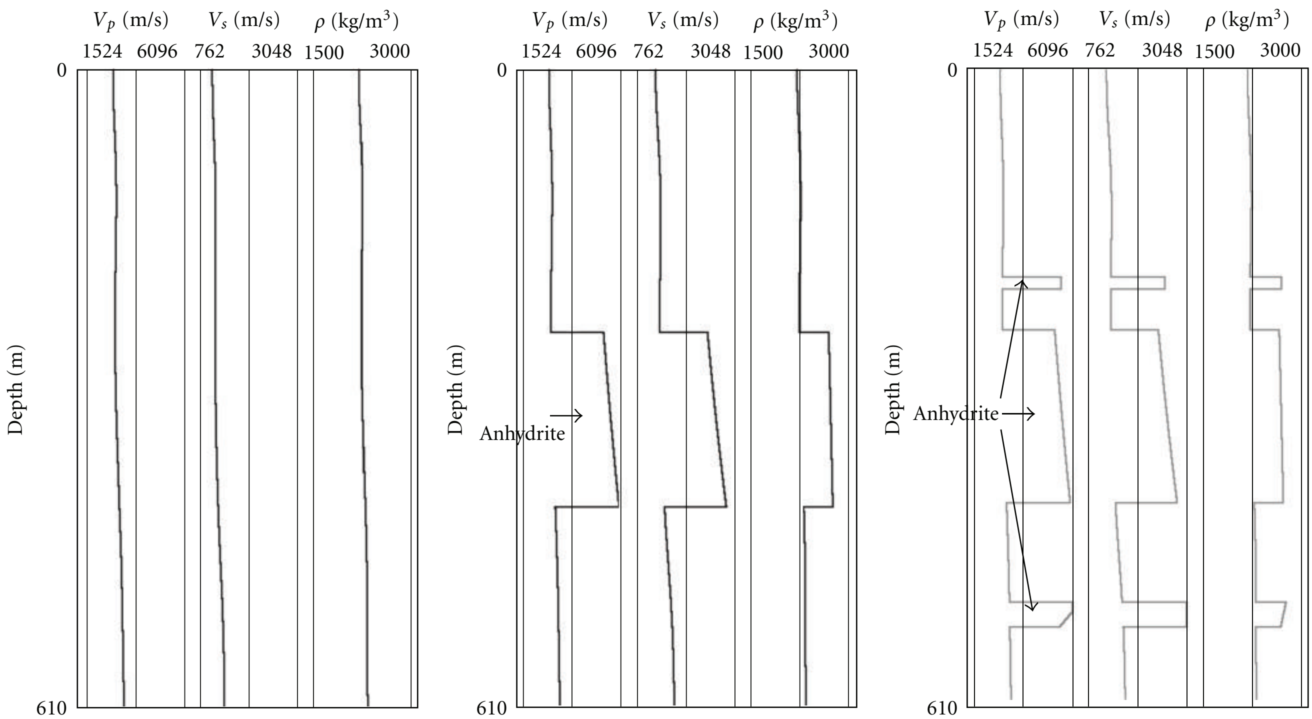

(a) Model a

(b) Model b

(c) Model b

Figure 6: The three different versions of the 1D models shown in Figure 5, used to understand the effect of shallow anhydrite layers. Model a—no anhydrite layer, Model b—one anhydrite layer, and Model c—three anhydrite layers.

The average porosity of this sand is 17% and the permeability is around 50 md.

3. Elastic Modeling

Seismic modeling is done to compute synthetic seismograms for a given geologic model. There are different methods for simulating seismic wave propagation including ray tracing, reflectivity, integral-equation, finite difference, finite element, and so forth, [36–38]. There are also hybrid approaches which combine two or more of the above methods [39]. In this study, we have used the finite difference technique for computing the elastic wave equation and generating the synthetic seismograms [40, 41]. It is necessary to compute synthetic gathers for horizontal and vertical source-receiver combinations in order to compare the seismic signatures of different wave modes (P-, PS-, and S-waves). Finite difference modeling simulates the full wavefield while preserving the amplitudes and phases. It helped in understanding the strong effect of multiples due to shallow high velocity anhydrite layers. Finite difference modeling is considered to be expensive in terms of computing time and memory, but since we are using a 1D model, this was not a problem. 2D multicomponent gathers are generated using this 1D model. The grid size is 4.572 m × 4.572 m and the model size is kept large enough to avoid interference between side reflections from the boundary and the main events. Finite difference modeling also allows us to look at the propagated wave field at certain time by taking snapshots.

4. Model Building

Well logs from a well with dipole sonic logging have been used for elastic parameters. Figure 3 shows the P-velocity (V_p), S-velocity (V_s), and density (ρ) logs from that well. There are three anhydrite layers between the surface and 550 m, and the reservoir Morrow A sandstone is at a depth of 1875 m. The close-up of Morrow level in Figure 3 shows the strong S-wave velocity contrast between Morrow shale and A sandstone as compared to P-wave velocity contrast. This leads to good amplitude versus angle (AVA) response for S-wave at the top of Morrow A sandstone as compared to P-wave and PS-wave (Figure 4). The well logs shown in Figure 3 are blocked, smoothed, and modified to have a detailed understanding of seismic response at the Morrow level. The three models (Figure 5) built to understand the Morrow A sandstone AVO response and interference effects are the following.

Model 1: only Morrow A sandstone interval,

Model 2: Morrow A sandstone with one limestone layer below,

Model 3: Morrow A sandstone with Atoka limestone above and one limestone layer below.

The presence of shallow high velocity anhydrite layers limits the incident angle and offset at the top of Morrow A sandstone. The rays are critically refracted at small angles of incidence at the top of the high velocity anhydrite layers,

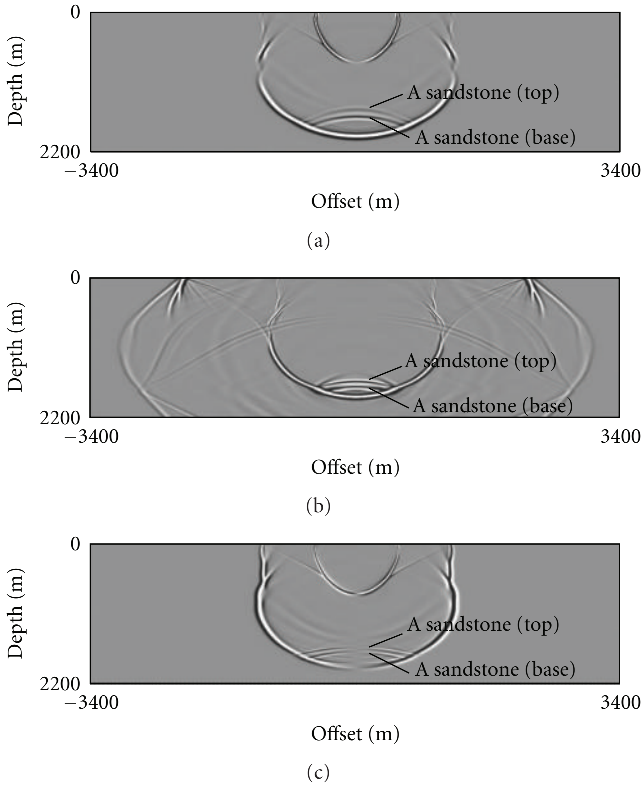

Figure 7: Wave propagation snapshots for (a) P-wave, (b) S-wave and (c) PS-wave using Model 1a. We observe that S-wave shows a stronger Morrow A sandstone response as compared to P- and PS-wave.

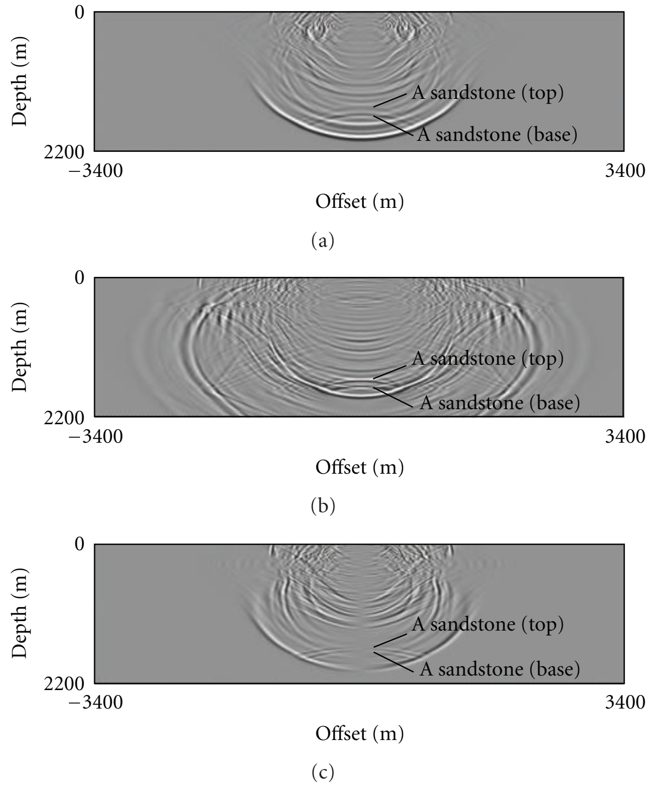

Figure 8: Wave propagation snapshots for (a) P-wave, (b) S-wave and (c) PS-wave using Model 1c. We observe that amplitude of multiples due to shallow anhydrite layers is stronger than the reflection from the top of Morrow A sandstone in P- and PS-wave snapshot. Whereas the Morrow A sandstone response is stronger than the amplitude of multiples in S-wave snapshot.

and hence, we do not get large angles and offsets for the target reservoir. The reverberations due to these high velocity anhydrite layers create strong multiples which have an adverse effect on data and are discussed in next section. These shallow layers vary in thickness and lithology laterally. To have a better understanding of the effect of these shallow anhydrite layers, Models 1, 2, and 3 are further divided into following three models (Figure 6).

Model a: No anhydrite layer,

Model b: One anhydrite layer,

Model c: Three anhydrite layers.

5. Morrow A Seismic Signature

Gathers are calculated for horizontal and vertical sources, and both the horizontal and vertical components are recorded. To have a close match with the field data, in this full waveform modeling study, all receiver components record different types of waves and none of the source-receiver combinations produce a pure P-, PS-, or S-wave records. But for simplicity, in this paper, we will refer to vertical source-vertical receiver recording as P-wave, vertical source-horizontal receiver recording as PS-wave, and horizontal source-horizontal receiver recording as S-wave recording, because these are the dominant waves in these source-receiver combinations. An 18 Hz Ricker wavelet is used for P-wave modeling and a 13 Hz Ricker wavelet is used for S- and PS- wave modeling. These wavelets are chosen based on the dominant frequency observed at Morrow level in real data.

5.1. Wave Propagation Snapshot. We know from well logs that the acoustic impedance contrast between Morrow sandstone and encasing shale is weak as compared to the shear impedance contrast. The wave propagation snapshots for P-wave, PS-wave, and S-wave confirm these observations. Figures 7(a) and 7(c) show the weak P-wave and PS-wave response at the top of Morrow A sandstone respectively, as compared to the strong S-wave response (Figure 7(b)), which is similar to the observation in Figure 5. This is for the case of Model 1a, that is, just the Morrow A sandstone with no anhydrite layer. Figures 8(a), 8(b), and 8(c) show the P-wave, S-wave and PS-wave propagation snapshot for Model 1c, that is, just the Morrow A sandstone with three anhydrite layers. The amplitude of multiples due to anhydrite layers is stronger than the reflection from the top of Morrow A sandstone in case of P- and PS-wave (Figures 8(a) and 8(c)), whereas for S-wave, the Morrow A sandstone response is stronger than the amplitude of multiples (Figure 8(b)).

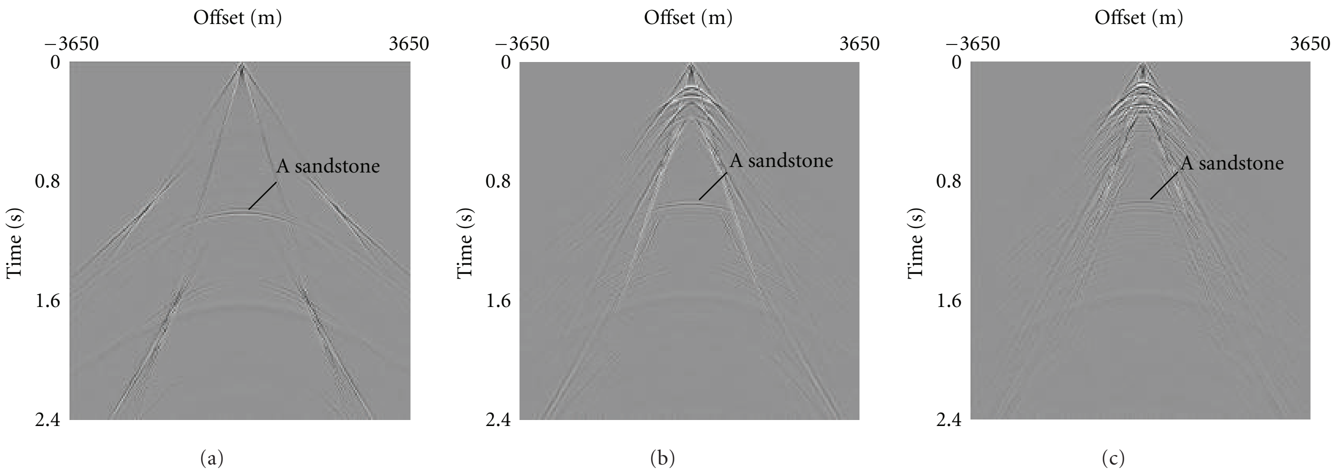

FIGURE 9: P-wave gather for the case of (a) Model 1a, (b) Model 1b, and (c) Model 1c, shows that the amplitude of multiples due to shallow anhydrite layers is comparable to the amplitude of primary reflections.

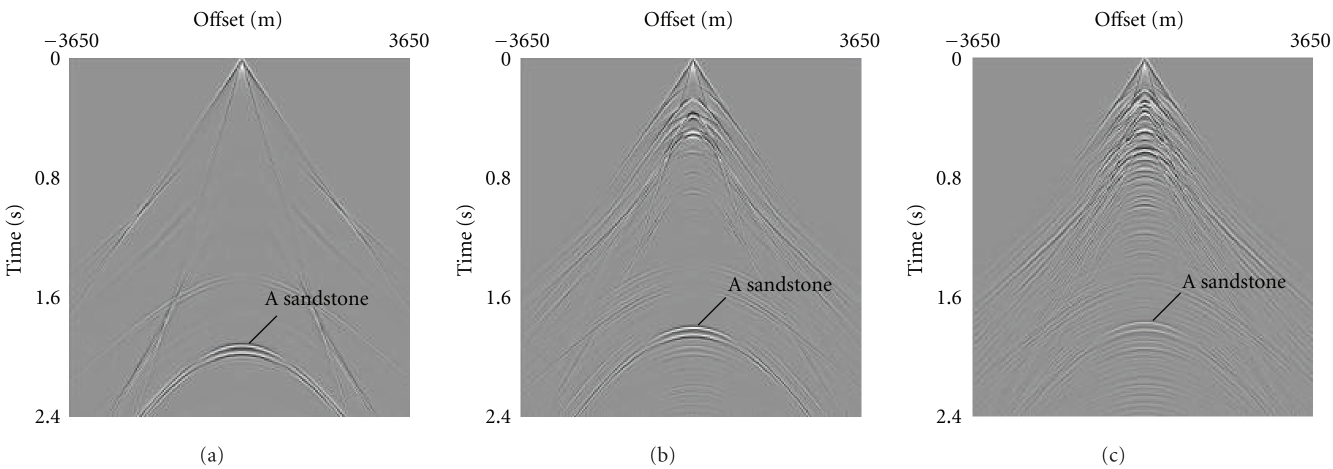

FIGURE 10: S-wave gather for the case of (a) Model 1a, (b) Model 1b, and (c) Model 1c, shows that the primary reflection amplitude is stronger than the amplitude of multiples.

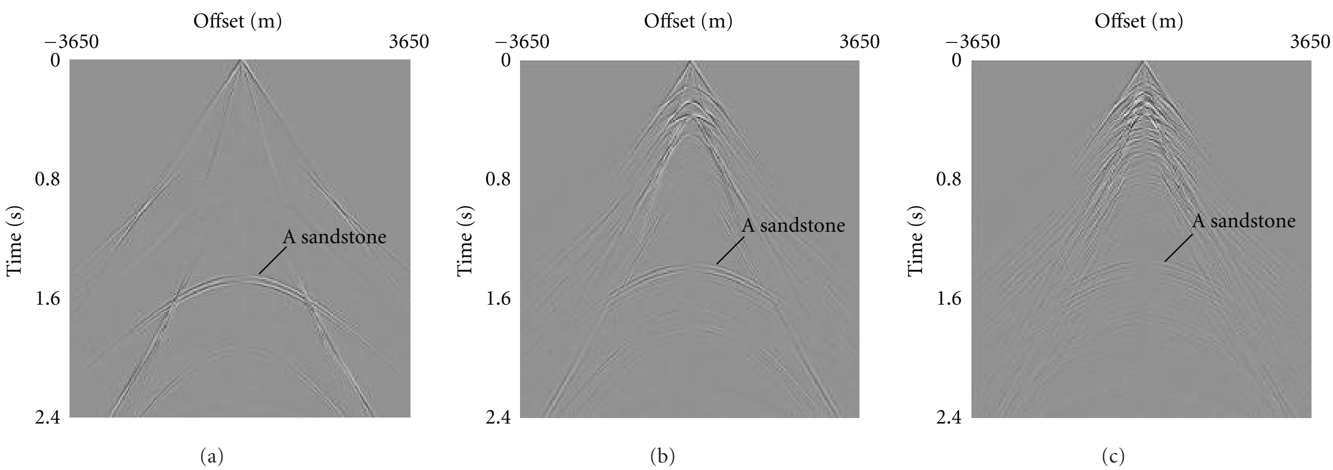

FIGURE 11: PS-wave gather for the case of (a) Model 1a, (b) Model 1b, and (c) Model 1c, shows that the amplitude of multiples due to shallow anhydrite layers is comparable to the amplitude of primary reflections.

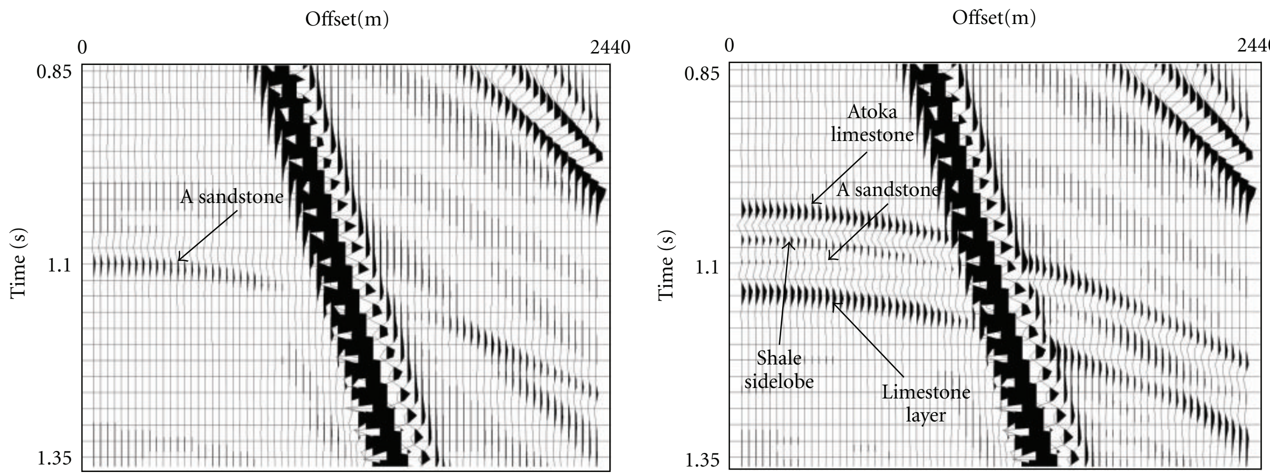

(a) (b)

FIGURE 12: (a) P-wave gather for Model 1a shows a Class II AVO anomaly at the top of Morrow A sandstone where a small peak changes into trough with offset. (b) The P-wave gather for Model 3a shows that the peak at the top of Morrow A sandstone is interfered with the side lobe of Morrow shale and bottom limestone layer. This gives a peak doublet at near offsets which changes to a single peak at far offsets.

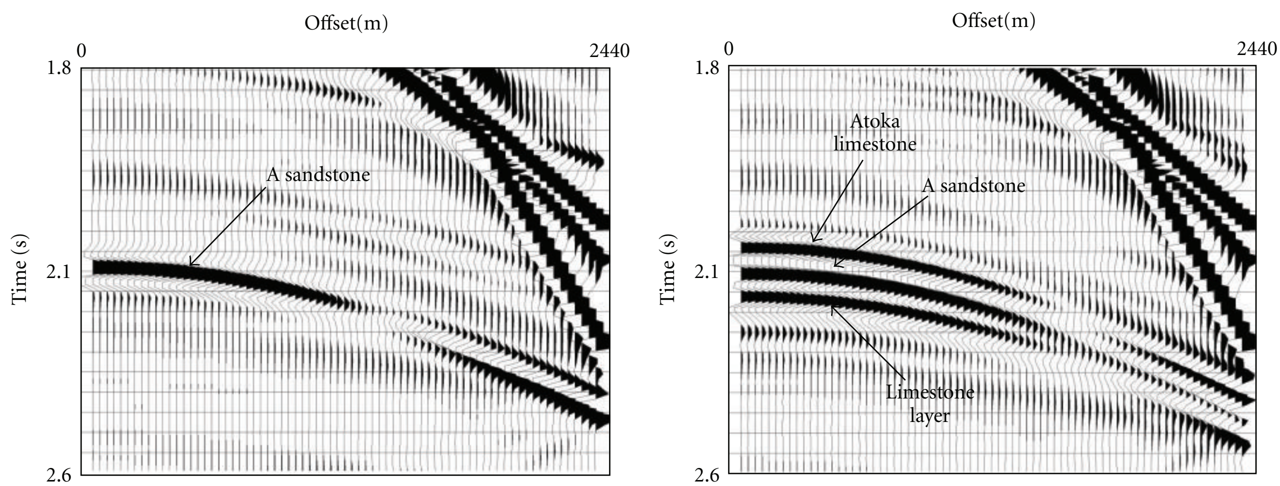

(a) (b)

FIGURE 13: (a) S-wave gather for Model 1a shows a strong peak response at the top of Morrow A sandstone which changes to trough with offset. (b) The S-wave gather for Model 3a shows that even in the presence of overlying shale and bottom limestone layer the Morrow A sandstone shows a distinct high amplitude AVO response.

5.2. Effect of Multiples. Internal multiples ringing in the shallow anhydrite layers have a significant effect on P-wave, PS-wave, and S-wave gathers. To have a better understanding of the effect of multiples on the three wave modes (Figures 9, 10, and 11), synthetic gathers are generated using Models 1a, 1b, and 1c. Since the acoustic impedance contrast between Morrow sandstone and shale is weak, the reverberations due to the anhydrite layers overshadow the Morrow A sandstone response in P-wave (Figure 9(c)). Melvin [42] describes the adverse effects of multiples in P-wave data at Postle Field and suggests ways to correct them. These multiples do not affect the S-wave gather significantly, since the Morrow A sandstones have a distinct high amplitude response compared to the weak reflectivity of multiples (Figure 10(c)). The PS-wave reflection from the Morrow A sandstone is also weak. Thus, the reverberations due to anhydrite layers overshadow the Morrow A sandstone response in PS-wave gather (Figure 11(c)). The data gets badly affected with increasing anhydrite layers.

5.3. Interference Effect. Figures 12, 13, and 14 show the zoomed sections from the P-wave, S-wave, and PS-wave gathers respectively. Models 1a and 3a with 19.5 m sandstone thickness have been used for understanding Morrow A sandstone AVO response and interference effects. For Model 1a, the P-wave gather shows a weak class II AVO response at the top of Morrow A sandstone (Figure 12(a)), where the peak changes to trough with offset. This is similar to

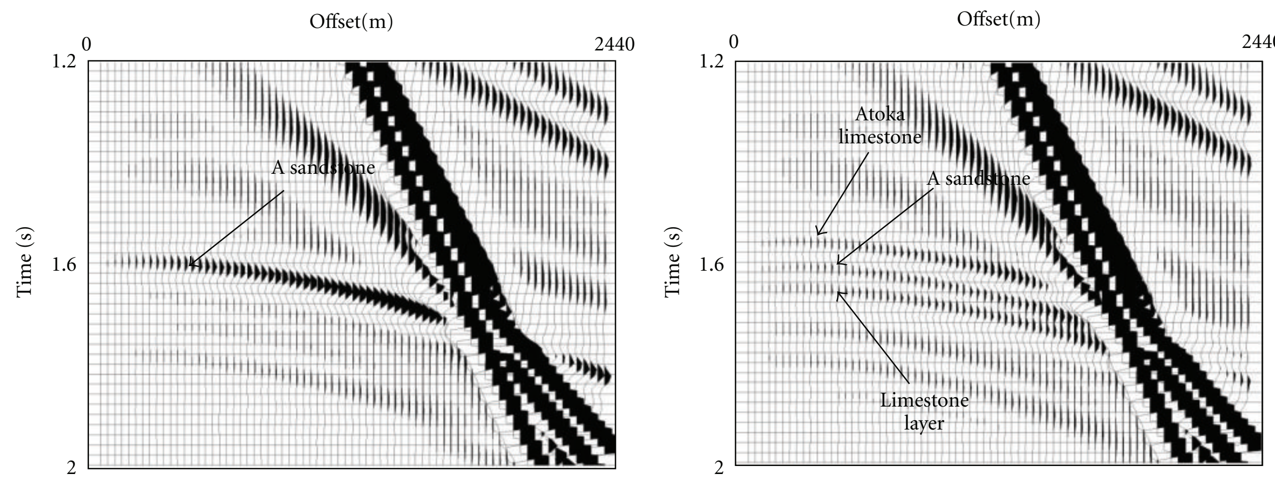

(a) (b)

Figure 14: (a) PS-wave gather for Model 1a shows increasing peak amplitude with offset at the top of Morrow A sandstone. (b) The PS-wave gather for Model 3a shows that the peak response at the top of Morrow A sandstone is weakened due to the interference with Morrow shale and bottom limestone layer.

the P-wave AVA response shown in Figure 4. Figure 12(b) shows the interference effect of the Morrow shale and the underlying limestone layer on the Morrow A sandstone AVO response. It leads to a peak doublet with side lobe of Morrow shale showing stronger amplitude. With increasing offset the peak doublet changes into a single peak which makes P-wave AVO analysis difficult. Stacking will also give a peak doublet for Morrow A sandstone, having inseparable peaks (observed in real P-wave stack, Figure 18(a)). This makes horizon picking difficult and P-wave interpretation challenging.

The change in rigidity between the reservoir sandstone and surrounding shale causes a strong seismic expression on the S-wave data. For Model 1a, the response of Morrow A sandstone is a peak which turns to trough with increasing offsets (Figure 13(a)) and is similar to the S-wave AVA response shown in Figure 4. Even for Model 3a which has overlying shale and an underlying limestone layer, the S-wave gather shows a distinct high amplitude AVO response for Morrow A sandstone (Figure 13(b)). The synthetic gather shows that S-wave AVO can be very useful in characterizing the A sandstones. The real data S-wave stack (Figure 18(b)) shows a distinct high amplitude peak for Morrow A sandstone which makes interpretation simpler. For Model 1a, the PS-wave shows a weak peak response at the top of A sandstone and the amplitude increases with offset (Figure 14(a)). This is similar to the PS-wave AVA response shown in Figure 4. The peak response due to Morrow A sandstone is weakened due to the interference effect of Morrow shale and bottom limestone layer (Figure 14(b)).

The reservoir sandstone thickness varies from 0–30 m in the study area. Wedge modeling is done to understand the effect of changing sand thickness on different wave components. The sandstone thickness in the model is changed from 0 to 32.5 m at an increment of 6.5 m to understand the interference effect. P-wave, S-wave, and PS-wave gathers are displayed side by side in Figure 15 to compare the AVO responses for changing sand thicknesses. When the Morrow A sandstone is absent, the P-wave gather shows a weak peak response from the side lobe of Morrow shale. As the sand thickness increases, we observe a peak doublet after 13 m of sandstone thickness. The peak amplitude of this doublet increases with increasing sand thickness.

S-wave gather shows separate peak response even till 6.5 m of A sandstone. The peak amplitude for the S-wave event increases with increasing sandstone thickness. In the PS-gather, the peak at the top of A sandstone starts interfering with the peak of bottom limestone layer as the thickness drops down to 13 m sandstone, making interpretation difficult. For PS-waves also, the peak amplitude increases with increasing sandstone thickness. So, it is observed that with P-waves and PS-waves, it is difficult to detect A sandstones less than 13 m thick, whereas the S-wave gather shows a distinct high amplitude response even for 6.5 m sandstone thickness, which is very useful since the average thickness of A sandstone in the study is approximately 10 m.

6. Field Data Results

The Reservoir Characterization Project in Colorado School of Mines acquired and processed a 3D-9C survey in Postle field for reservoir characterization of Morrow A sandstones and for monitoring a CO_2 flood. The study area is nearly 16.2 sq$\cdot$ km with 16 shot and receiver lines (Figure 16). The shot lines are in E-W direction with 268.2 m spacing and the receiver lines are in N-S direction with 268.2 m spacing. The shot point and receiver point interval is 33.5 m and the bin size is 33.5 m $\times$ 33.5 m. Data acquisition was done by keeping all the receivers active for each shot. While processing, the pre-stack shear wave data is rotated using Alford rotation [43], with fast shear (S1) in the direction of N105E. This fast

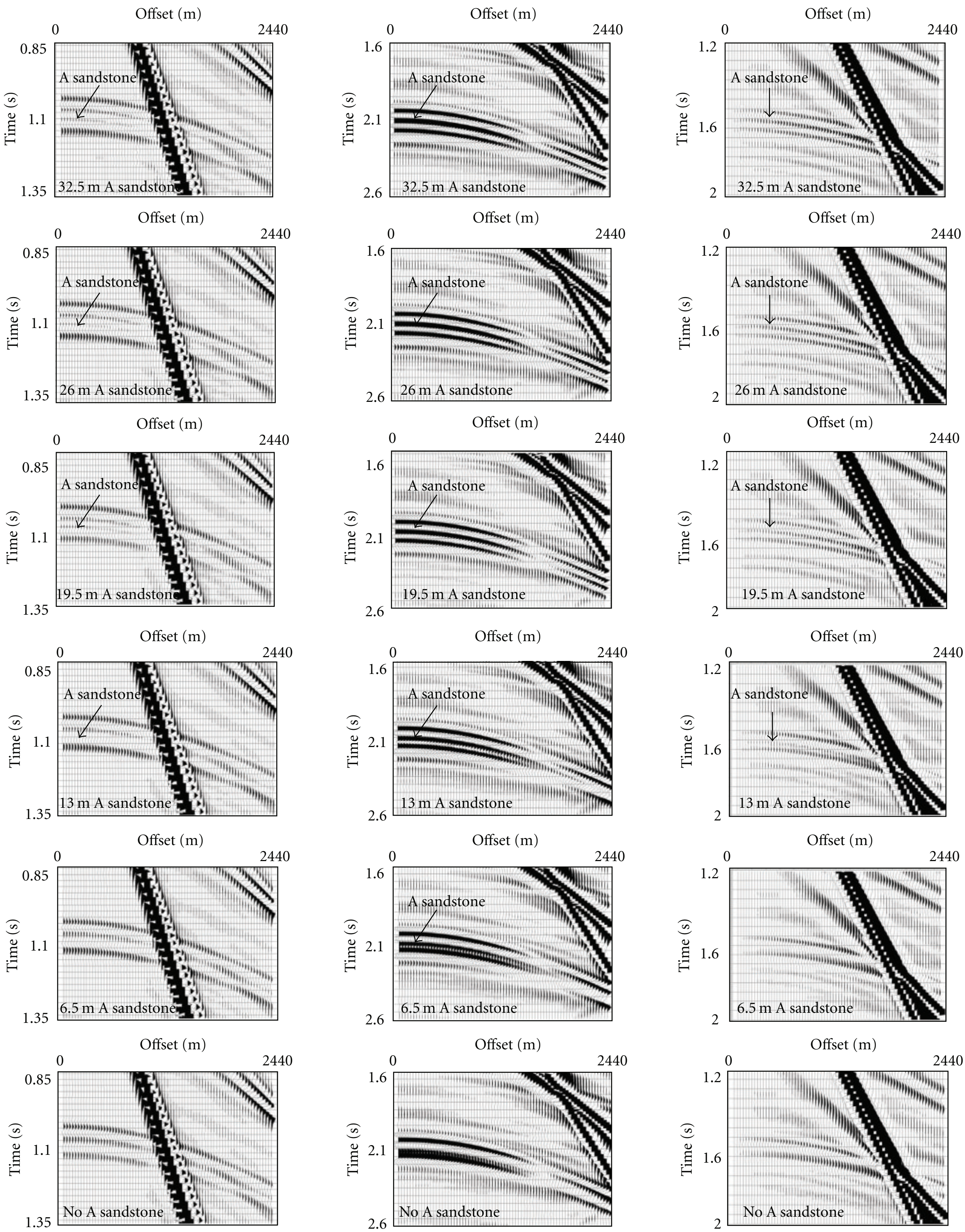

Figure 15: P-wave gathers (left), S-wave gathers (center) and PS-wave gathers (right) generated using Models 3a, with changing A sandstone thickness from 0 to 32.5 m. The synthetic gathers show that it is difficult to detect less than 13 m sandstone thickness using P-waves, since the peak doublet is absent. In PS-wave gather, the separate peak response is not present for 13 m of A sandstone thickness. The S-wave gather shows a distinct peak response even for 6.5 m of A sandstone thickness.

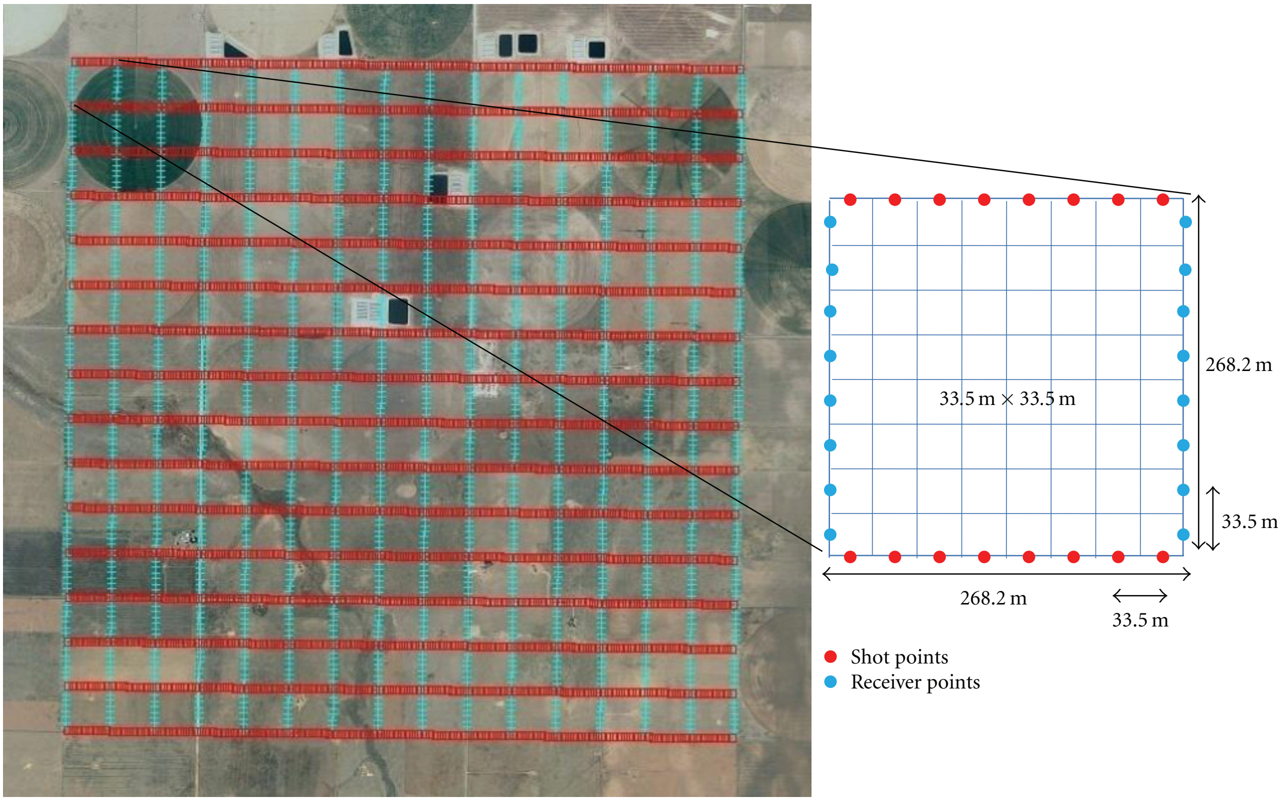

Figure 16: Acquisition parameters. Shot points are shown by red dots and receiver points are shown by blue dots. There are 16 shot lines in E-W direction and 16 receiver lines in N-S direction. Both shot and receivers point spacing is 33.5 m, and the data is binned at 33.5 m × 33.5 m.

shear wave direction or the direction of maximum horizontal stress has been obtained from well log information.

The P-wave gather in Figure 17(a) shows the AVO response similar to the synthetic gather (Figure 12(b)) around 1.07 s, where a peak doublet at near offset changes to single peak with increasing offset. The S1-wave gather in Figure 17(b) also shows an AVO response similar to the synthetic gather (Figure 13(b)) around 2.08 s, where a strong peak changes to trough with increasing offset. Figures 18(a) and 18(b) shows the P- and S1-wave stacks, respectively, along an inline passing through the well used for elastic modeling. Gamma Ray log from that well is shown by red curve in the stacks. The dip of the reflectors in P-wave stack and S1-wave stack is different, because the statics for each stack was computed independently. In the P-wave stack (Figure 18(a)), the horizon picked in blue is the Morrow shale, and the strong peak reflector above is Atoka limestone. Due to the interference with the side lobe of Morrow shale, Morrow A sandstone shows a peak doublet below Morrow shale trough. There are other Morrow sandstone layers below, but these cannot be seen clearly in the P-wave stack because of the weak acoustic impedance contrast. In the S1-wave stack (Figure 18(b)) the horizon picked in blue is the Morrow shale and the reflector above is Atoka limestone. In the S1-wave stack, the Morrow A sandstone has a strong peak amplitude below the Morrow shale trough. Due to the addition of static correction, the Morrow sandstone reflector in S1-wave stack appears around 2.25 s as compared to 2.08 s in gather. Owing to the good shear impedance contrast between Morrow sandstone and shale we can observe strong reflectors below Morrow A sandstone as well, indicating presence of other sandstone bodies below. This can help in future investigation of deeper reservoir possibilities.

P- and S1-amplitude maps were extracted along the Morrow A peak and are shown in Figures 19(a) and 19(b), respectively. Due to the adverse effect of multiples in the converted-wave data, PS-amplitude map has not been shown here. Those data need further processing to remove that noise. For the P-wave amplitude map, the sum of positive samples is computed in a 0.035 s window centered on Morrow A peak. For S1-wave the window is 0.05 sec. The window size for both P and S1-wave is chosen so that the complete Morrow A sandstone peak amplitude is considered. The well pattern is overlaid on top of the amplitude maps, since these are the places were A sandstone have been encountered. The wells drilled outside this pattern have not encountered Morrow A sandstone, hence we expect to see high amplitudes mainly in this well pattern area. The high amplitudes in S1-wave map lie mostly within the well pattern as compared to P-wave map. Thus, the well pattern matches better with the sandstone distribution map obtained from S1-wave stack as compared to P-wave stack. Figure 20 shows the gross sandstone thickness map constructed by picking the top and base of A and A1 sandstone in well

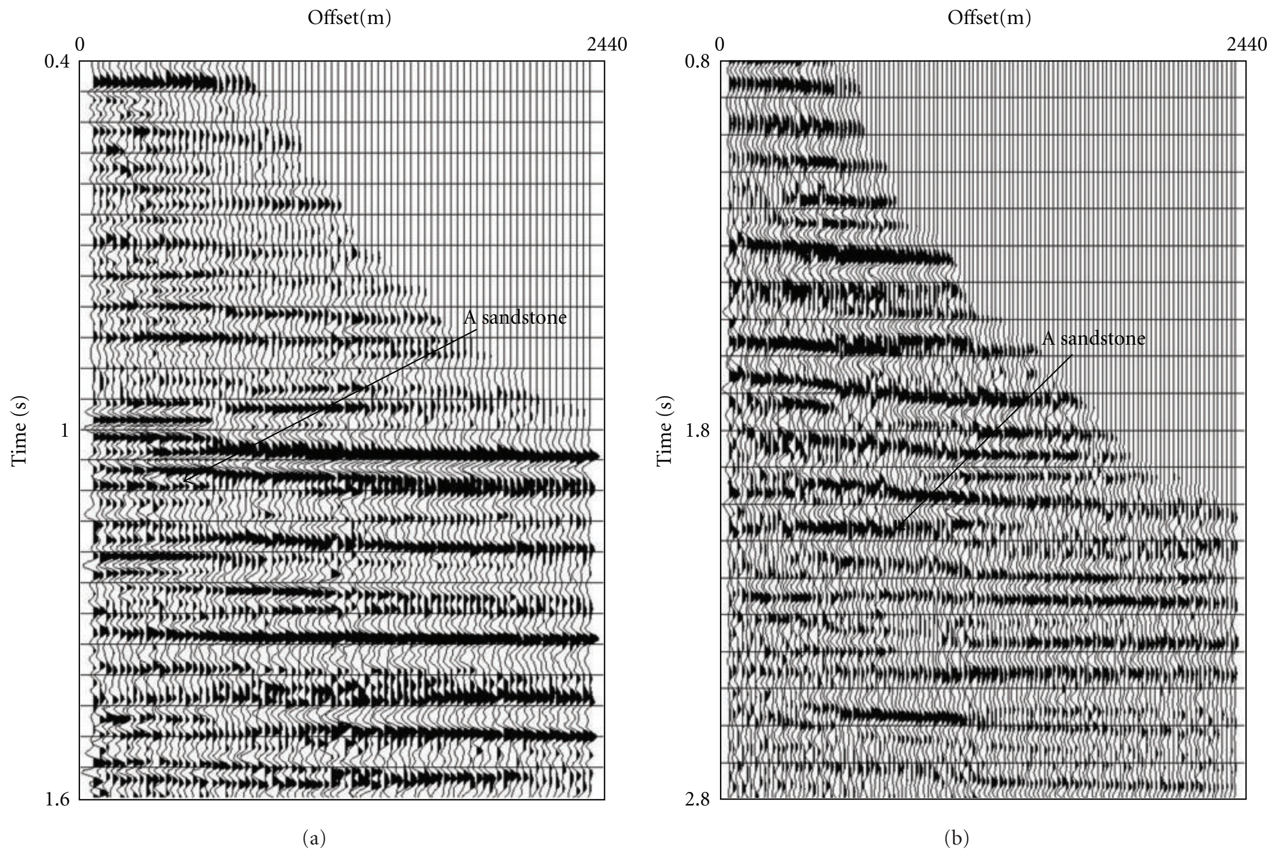

FIGURE 17: (a) P-wave gather shows a peak doublet at the top of Morrow A sandstone (1.07 s) which changes to single peak at far offsets. (b) S1-wave gather shows a peak response at the top of Morrow A sandstone (2.08 s) changing to trough with offset. The AVO response in real data P- and S1-wave gathers matches with the synthetic gather AVO response shown in Figures 12(b) and 13(b).

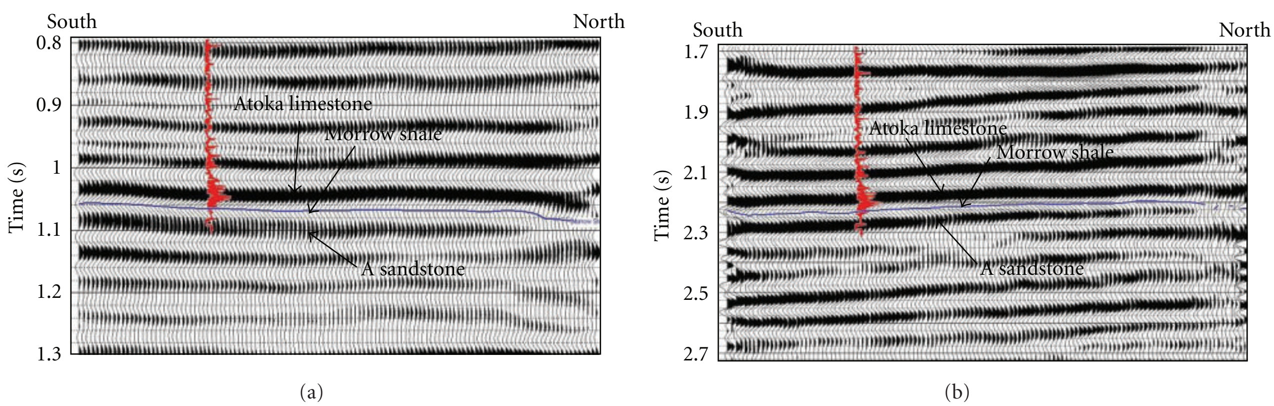

FIGURE 18: The above sections are (a) P-wave stack and (b) S1-wave stack along an inline passing through the well used for modeling study. The Morrow A sandstone peak interferes with the side lobe of shale to give a peak doublet in P-wave stack. The S1-wave stack has a distinct Morrow A sandstone peak response. The S1-wave stack also shows some high amplitude sand layers below Morrow A which are not clearly evident in P-wave stack.

logs and interpolating the calculated thickness between well locations (courtesy Whiting Petroleum). S1-amplitude map shows a trend similar to the gross A sandstone thickness map (Figure 20(a)), except for the high amplitude anomalies in the west (shown in black oval). The high amplitudes in the west may be due to Morrow A1 sandstone (Figure 20(b)), but further investigation is needed to confirm this. The Morrow A1 sandstone is another sandstone layer lying 3–15 meters below A sandstone and is prominent in western part of the study area. So, in the western part, where there is no Morrow A sandstone, we may get high amplitudes due to the presence of Morrow A1 sandstone.

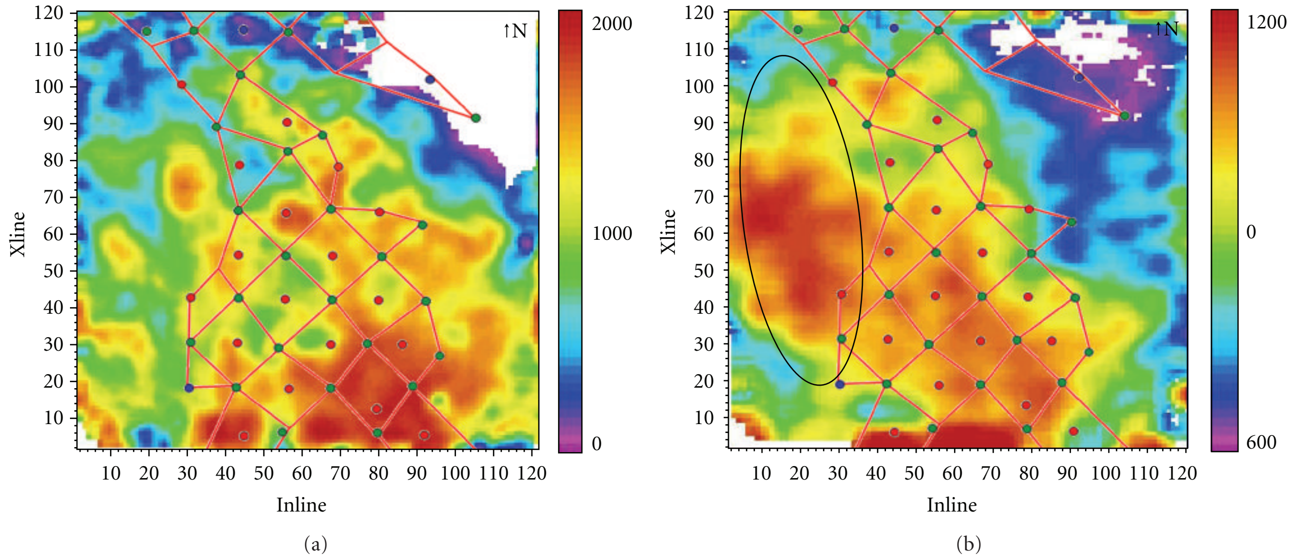

Figure 19: (a) P-wave amplitude map and (b) S1-wave amplitude map are shown with well pattern overlaid on them (green dots represent producer wells; red dots represent injector wells). The amplitude map is obtained by computing sum of positive samples in a 0.035 s window centered around peak doublet for P-wave and 0.05 s window centered around peak for S1-wave. The S1-wave amplitude shows better match with the well pattern, except in the western part of the study area (shown by black oval) where there is presence of Morrow A1 sandstone (Figure 20(b)).

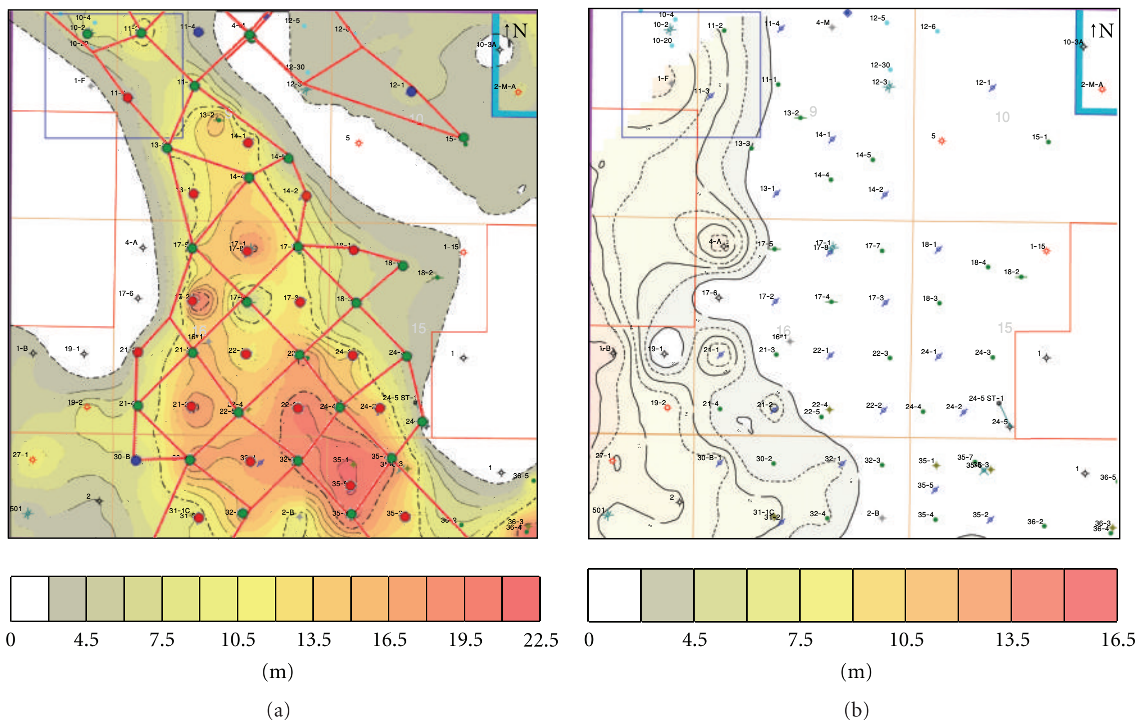

Figure 20: Gross sandstone thickness maps for (a) Morrow A sandstone and (b) Morrow A1 sandstone (courtesy Whiting Petroleum). The star in the map is the well used for elastic modeling.

The P- and S1-amplitude values are computed in a 4 × 4 (inline × xline) radius around the well locations in high fold area and compared with the gross A sandstone thickness value at each well location (Figure 21). Elastic modeling showed that for both P- and S-waves the peak amplitude increases with increasing A sandstone thickness. Figure 21 proves that the P- and S1-ampitude values increase with increasing A sandstone thickness. It also shows that S1-amplitude map has better correlation (correlation coefficient 0.60) with gross A sandstone thickness as compared

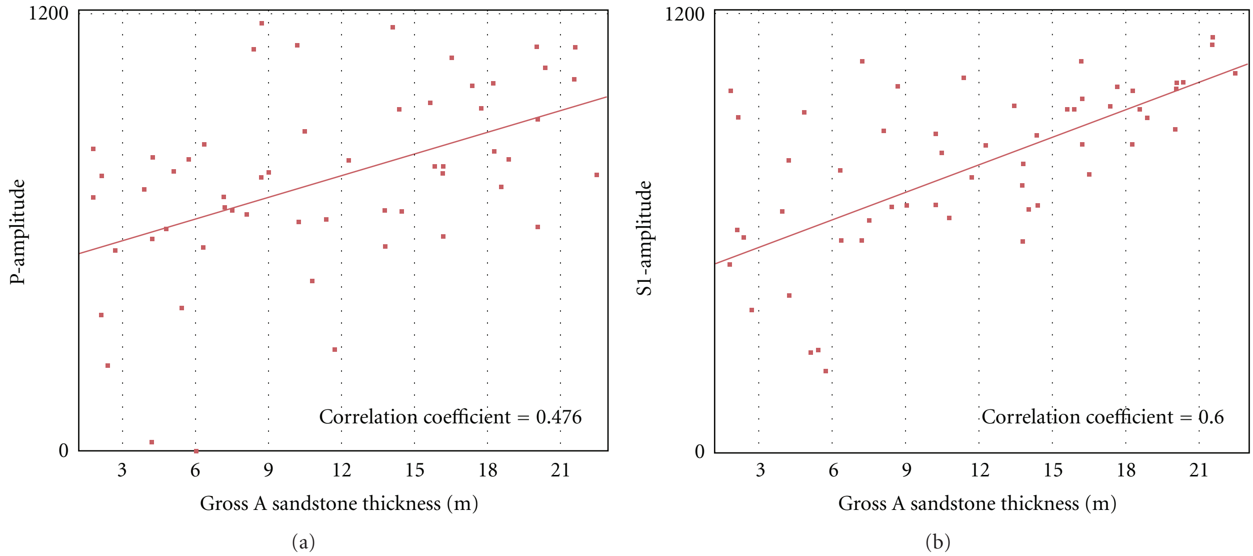

Figure 21: S1-wave amplitude map has a better correlation to gross A sandstone thickness than the P-wave amplitude map. For the S1-wave amplitude map, the correlation is not good when the sandstone thickness is less than 6.5 m, whereas the P-wave amplitude map does not show good correlation even for thicker sandstones.

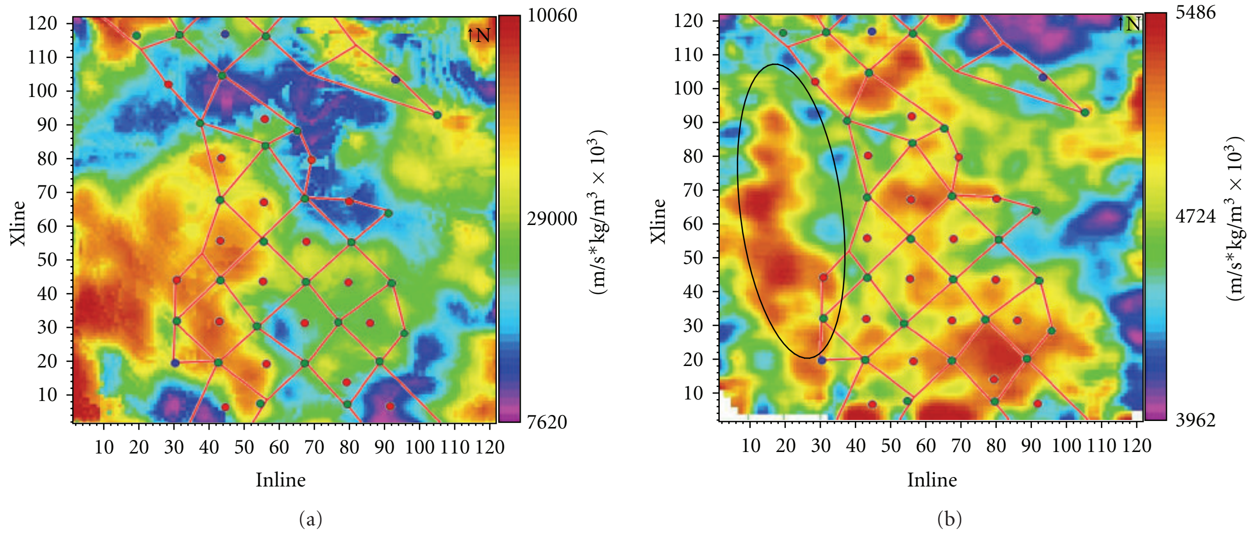

Figure 22: (a) P-wave impedance map and (b) S1-wave impedance map (right) are shown with well pattern overlaid on them (green dots represent producer wells; red dots represent injector wells). For P-waves, the impedance map is obtained by computing rms amplitude in a 0.009 s window centered on Morrow A sandstone. For S1-waves, the impedance map is obtained by computing rms amplitude in a 0.01 s window centered on Morrow A sandstone [35]. The S1-wave impedance shows better match with the well pattern. The high impedance in the west part of the study area (shown by black oval) ties with the presence of A1 sandstone (Figure 20(b)).

to P-amplitude map (correlation coefficient 0.476). The P-wave amplitude map does not show good correlation even for thicker sandstones and the correlation is almost same for all sandstone thicknesses. The S1-amplitudes map has good correlation for thicker sandstones and the correlation drops down mainly below 6.5 m of sandstone as predicted by the modeling. Thus, S1-amplitude map is a good indicator of Morrow A sandstone distribution and thickness.

Pinto [35] performed post stack impedance inversion on P- and S1-wave stacks and the results are shown in Figure 22. Comparing the P-impedance map (Figure 22(a)) with well pattern and gross A sandstone thickness map suggests that it is unable to map Morrow A noticeably. The failure of P-impedance map to detect the A sandstones is due to weak impedance contrast between Morrow shale and A sandstone, and also due to the interference between the A sandstone peak with the side lobe of Morrow shale and underlying limestone layer. Excluding the high impedance anomaly in the west, the S1-impedance map (Figure 22(b)) shows good sandstone distribution and ties well with the overlaid well pattern and the gross A sandstone distribution shown in Figure 20(a). The high impedance in the west part of the study area matches with the gross A1 sandstone distribution shown in Figure 20(b).

CO_2 flooding in the study area has proceeded towards the north part of the block and it is very important to find the sandstone distribution in the north. The S1-impedance map helps us in mapping sands in the north part of the block, where P-impedance map completely fails. This can be very useful in future well planning and increased production.

7. Conclusions

There are many examples like Postle Field in the world which have been producing for many decades but still have lot of reserves left to be exploited. These prolific reservoirs are important exploration plays, yet the reservoirs are difficult to detect using conventional P-wave seismic. New technologies and methods can help in exploiting these reserves. Shear wave data has the potential to revive and extend the life of mature fields like Postle. It helps in imaging the sandstones and also monitoring the enhanced oil recovery. This is because S-waves are more sensitive to pressure changes than are P-waves.

To date, mostly compressional wave studies have been done to characterize Morrow sandstones, with limited modeling studies. The full waveform modeling shows that S-waves are better than P- or PS-waves for Morrow sandstone detection. This study helped in understanding the Morrow A sandstone AVO response for different wave modes. The modeled gathers for P-, S-, and PS-wave show that stronger amplitudes correspond to thicker A sandstone accumulations. Modeling helped in understanding the interference effect due to the overlying shale and a limestone layer below. It also helped in understanding multiples caused by shallow anhydrite layers. S-wave data are commonly used for fracture mapping but this study shows their use in detecting thin reservoir sandstones. The present modeling study is tied to the results from field data showing how shear wave data have important implications for oil exploration and development in areas where P-wave data is unsatisfactory. The shear wave rotation analysis and data processing is still going on, and we hope to get better results from P-, PS-, and S-wave data interpretation in future.

Acknowledgments

The authors would like to thank BP America for providing the modeling software for this study and Mike O'Brien for helping us use the software. We would sincerely thank the Reservoir Characterization Project Sponsors and students for their support and encouragement. Special thanks to Whiting Petroleum for providing the multicomponent data and Fairfield Industries for processing it.

References

[1] R. P. Sorenson, "A dynamic model for the Permian Panhandle and Hugoton fields, western Anadarko basin," *American Association of Petroleum Geologists Bulletin*, vol. 89, no. 7, pp. 921–938, 2005.

[2] D. D. Rice, C. N. Threlkeld, and A. K. Vuletich, "Character, origin and occurrence of natural gases in the Anadarko basin, southwestern Kansas, western Oklahoma and Texas Panhandle, U.S.A," *Chemical Geology*, vol. 71, no. 1–3, pp. 149–157, 1988.

[3] J. R. Halverson, "Seismic expression of the upper Morrow sands, Western Anadarko Basin," *Geophysics*, vol. 53, no. 3, pp. 290–303, 1988.

[4] J. T. Noah, R. D. Teague, and G. Hofland, "Twin Morrow field: a case study," *The Leading Edge*, vol. 13, no. 1, pp. 25–30, 1994.

[5] M. Wiley, *Structural and stratigraphic controls on Morrow sandstone reservoir distribution from 3-D seismic data, Postle field, Texas county, Oklahoma*, M.S. thesis, Colorado School of Mines, Golden, Colo, USA, 2009, #T-6576.

[6] J. Gibson and S. Roche, "Multicomponent technology—reducing risk and creating opportunity," *Exploration and Production: The Oil and Gas Review*, pp. 1–7, 2005.

[7] J. Caldwell, P. Christie, F. Engelmark et al., "Shear waves shine brightly," *Oilfield Review*, vol. 11, no. 1, pp. 2–15, 1999.

[8] F. Engelmark, "Using converted shear waves to image reservoirs with low-impedance contrast," *The Leading Edge*, vol. 19, no. 6, pp. 600–603, 2000.

[9] M. K. MacLeod, R. A. Hanson, C. R. Bell, and S. McHugo, "The Alba field ocean bottom cable seismic survey: impact on field development," *The Leading Edge*, vol. 18, no. 11, pp. 1306–1312, 1999.

[10] G. F. Margrave, D. C. Lawton, and R. R. Stewart, "Interpreting channel sands with 3C-3D seismic data," *The Leading Edge*, vol. 17, no. 4, pp. 509–513, 1998.

[11] S. Knapp, N. Payne, and T. Johns, "Imaging through gas clouds: a case history in the Gulf of Mexico," in *Proceedings of the 71st Annual International Meeting*, pp. 776–779, SEG, 2002, Expanded Abstracts.

[12] F. Engelmark, "Using 4-C to characterize lithologies and fluids in clastic reservoirs," *The Leading Edge*, vol. 20, no. 9, pp. 1053–1055, 2001.

[13] S. Crampin, "Evaluation of anisotropy by shear-wave splitting," *Geophysics*, vol. 50, no. 1, pp. 142–152, 1985.

[14] M. A. Martin and T. L. Davis, "Shear-wave birefringence: a new tool for evaluating fractured reservoirs," *The Leading Edge*, vol. 8, no. 10, pp. 22–28, 1987.

[15] S. Crampin, "Anisotropy and transverse isotropy," *Geophysical Prospecting*, vol. 34, no. 1, pp. 94–99, 1986.

[16] S. Crampin, "Geological and industrial implications of extensive-dilatancy anisotropy," *Nature*, vol. 328, no. 6130, pp. 491–496, 1987.

[17] S. Crampin, "Nonparallel S-wave polarizations in sedimentary basins," in *Proceedings of the 58th Annual International Meeting*, pp. 1130–1132, SEG, 1988, Expanded Abstracts.

[18] S. Crampin, "The new geophysics: shear-wave splitting provides a window into the crack-critical rock mass," *The Leading Edge*, vol. 22, no. 6, pp. 536–549, 2003.

[19] H. B. Lynn and L. A. Thomsen, "Reflection shear-wave data collected near the principal axes of azimuthal anisotropy," *Geophysics*, vol. 55, no. 2, pp. 147–156, 1990.

[20] M. C. Mueller, "Using shear waves to predict lateral variability in vertical fracture intensity," *The Leading Edge*, vol. 11, no. 2, pp. 29–35, 1992.

[21] M. Rumon, *Shear wave time-lapse seismic monitoring of a tight gas sandstone reservoir, Rulison field, Colorado*, M.S. thesis, Colorado School of Mines, Golden, Colo, USA, 2006, #T-6187.

[22] M. Terrel, *Fracture permeability characterization at Weyburn field: from shear wave anisotropy through flow simulation*, Ph.D. thesis, Colorado School of Mines, Golden, Colo, USA, 2004, #T-5486.

[23] R. R. Stewart, J. E. Gaiser, R. J. Brown, and D. C. Lawton, "Converted-wave seismic exploration: applications," *Geophysics*, vol. 68, no. 1, pp. 40–57, 2003.

[24] T. Wilson, *Converted-Wave Morrow sandstone delineation, Eva South field, Texas County, Oklahoma*, M.S. thesis, Colorado School of Mines, Golden, Colo, USA, 2002, #T-5597.

[25] J. E. Blott, *Morrow valley fill sandstone reservoir characterization with 3D-3C seismology, Sorrento field, Colorado*, Ph.D. thesis, Colorado School of Mines, Golden, Colo, USA, 1997, #T-5006.

[26] D. C. Rampton, *The shear difference: improved characterization of a Morrow fluvial sandstone using the shear seismic response, Sorrento field, Southeast Colorado*, M.S. thesis, Colorado School of Mines, Golden, Colo, USA, 1995, #T-4759.

[27] T. L. Davis, "Dynamic reservoir characterization for high resolution connectivity mapping and conformance control. Morrow sandstone reservoir, Postle field, Oklahoma," Colorado School of Mines Proposal no. 8181, 2007.

[28] M. A. Zimmer, M. Prasad, G. Mavko, and A. Nur, "Seismic velocities of unconsolidated sands—part 1: pressure trends from 0.1 to 20 MPa," *Geophysics*, vol. 72, no. 1, pp. E1–E13, 2007.

[29] M. N. Toksöz, C. H. Cheng, and A. Timur, "Velocities of seismic waves in porous rocks," *Geophysics*, vol. 41, no. 4, pp. 621–645, 1976.

[30] P. Singh, T. Davis, and M. O'Brien, "Understanding Morrow A sands through elastic modeling," in *Proceedings of the 79th Annual International Meeting*, pp. 1252–1256, SEG, 2009, Expanded Abstracts.

[31] E. Arro, "Morrowan sandstones in the subsurface of the Hough area, Texas county, Oklahoma," *OCGS—The Shale Shaker Digest V*, vol. 15–17, pp. 16–30, 1965.

[32] D. W. Bowen and P. Weimer, "Regional sequence stratigraphic setting and reservoir geology of Morrow incised-valley sandstones (lower Pennsylvanian), eastern Colorado and western Kansas," *AAPG Bulletin*, vol. 87, no. 5, pp. 781–815, 2003.

[33] M. E. Henry and T. C. Hester, "Anadarko Basin Province (058)," 1995, http://certmapper.cr.usgs.gov/data/noga95/prov58/text/prov58.pdf .

[34] B. Rascoe Jr. and F. J. Adler, "Permo-Carboniferous hydrocarbon accumulations, Mid-Continent, U.S.A," *American Association of Petroleum Geologists Bulletin*, vol. 67, no. 6, pp. 979–1001, 1983.

[35] R. Pinto, "Vp/Vs: reservoir characterization project spring 2010 meeting presentation," Colorado School of Mines, 2010.

[36] J. M. Carcione, G. C. Herman, and A. P. E. ten Kroode, "Seismic modeling," *Geophysics*, vol. 67, no. 4, pp. 1304–1325, 2002.

[37] E. S. Krebes, "Seismic forward modeling," *CSEG Recorder*, pp. 28–39, 2004.

[38] G. F. Margrave and P. M. Manning, "Seismic modeling: an essential interpreter's tool," in *Proceedings of the CSEG National Convention*, 2004.

[39] I. Lecomte, H. Gjoystdal, A. Drottning, F. A. Maao, T. A. Johansen, and R. Bakke, "Efficient and flexible seismic modeling of reservoirs: a hybrid approach," *The Leading Edge*, vol. 23, no. 5, pp. 432–437, 2004.

[40] J. T. Etgen, "Finite-difference elastic anisotropic wave propagation," Stanford Exploration Project Report SEP-56, 1987.

[41] J. T. Etgen and M. J. O'Brien, "Computational methods for large-scale 3D acoustic finite-difference modeling: a tutorial," *Geophysics*, vol. 72, no. 5, pp. 223–230, 2007.

[42] C. E. Melvin, *The influence of P-wave multiple attenuation characterization of the Morrow A sandstone reservoir at Postle field, Texas county, Oklahoma*, M.S. thesis, Colorado School of Mines, Golden, Colo, USA, 2010.

[43] R. M. Alford, "Shear data in the presence of azimuthal anisotropy," in *Proceedings of the 56th Annual International Meeting*, pp. 476–479, SEG, 1986, Expanded Abstracts.